Plasmonics in Fluorescence and Microscopy

Zygmunt Gryczynski

Center for Commercialization of Fluorescence Technologies

University of North Texas Health Science Center at Fort Worth, TX

Fort Worth, November 2007

Jablonski Diagram

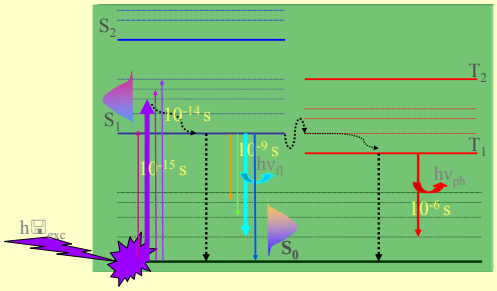

What is Fluorescence

Excitation and Emission

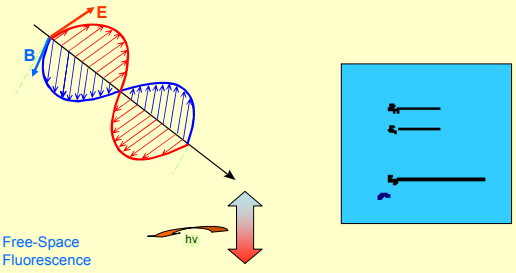

Free-Space Fluorescence

Sensitive to surrounding enviroment

New Directions in Fluorescence
Radiating Plasmons Model

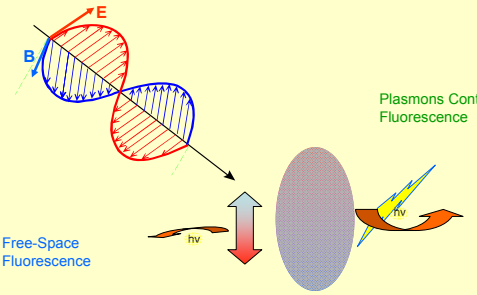

Recent Focus on Nanotechnology

Plasmons Enhanced Detection

Colloidal Scattering

Metal **E**nhanced **F**luorescence

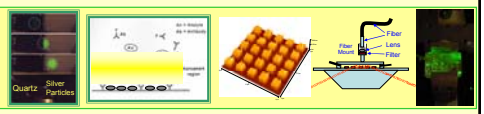

Surface **P**lasmon **C**oupled **E**mission

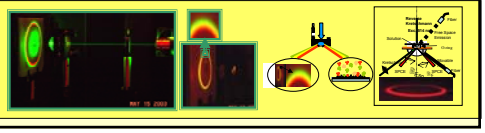

Optical Properties of Metal Colloids-
Gold Colloidal Spheres

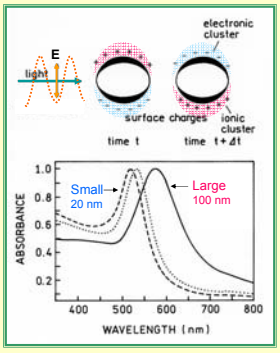

Can Intrinsic Particle Scattering Have Biomedical Applicability

Cell Labeling

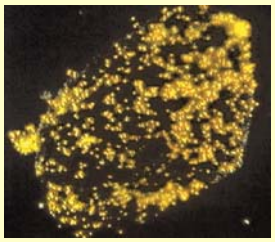

Photograph of epithelial buccal cells with 78-nm gold particles

J. Yguerabide and E. E. Yguerabide, Anal. Biochem. **262,** 137–156 (1998)

Polarized Light Scattering of Particles

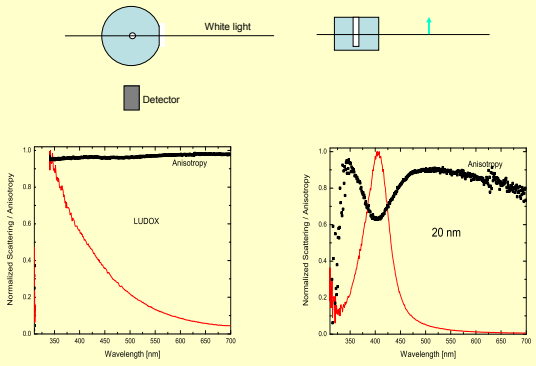

Different Colloids Concentrations

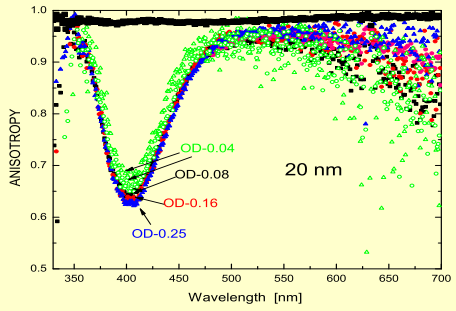

What About Wavelength or Solvent Viscosity

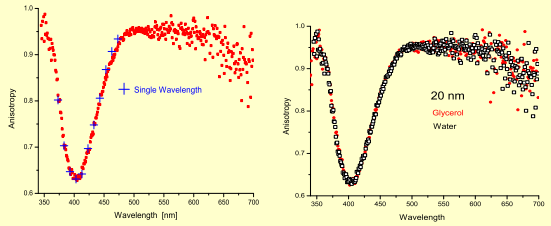

Application of Polarization Dependent Colloid Scattering

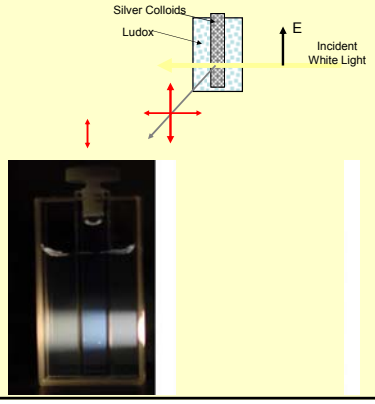

How to Explain Polarization Effect?

Polarization of a prolate spheroid in a uniform electric field

Laplace' equation of a potential V

$$\begin{cases} x = f\sqrt{\xi^2-1}\sqrt{1-\eta^2}\cos(\varphi) \\ y = f\sqrt{\xi^2-1}\sqrt{1-\eta^2}\sin(\varphi) \\ z = f\xi\eta \end{cases}$$

$$\begin{cases} \nabla^2 V = 0 \\ V = \sum_{n=0}^{\infty}\sum_{m=-n}^{n}\left[A_n^m P_n^m(\xi) + B_n^m Q_n^m(\xi)\right] P_n^m(\eta) e^{im\varphi} \end{cases}$$

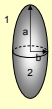

$$\begin{cases} \xi > 0 \\ 0 \le \eta < 1 \\ 0 \le \varphi < 2\pi \end{cases}$$

polarizabilities along the long and short axes

$$\alpha = f^3 \frac{4\pi\varepsilon_1(\varepsilon_2-\varepsilon_1)\xi_0}{3\left[\varepsilon_2\xi_0 Q_1'(\xi_0) - \varepsilon_1 Q_1(\xi_0)\right]} \qquad \beta = f^3 \frac{8\pi\varepsilon_1(\varepsilon_2-\varepsilon_1)\xi_0\sqrt{\xi_0^2-1}}{3\left[\varepsilon_1(\xi_0^2-1)Q_1'(\xi_0) - \varepsilon_2\xi_0 Q_1'(\xi_0)\right]}$$

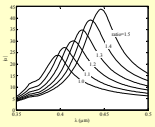

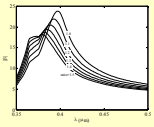

Interference of surface plasmon resonances causes enhanced depolarized light scattering from metal nanoparicles. (2007) Calander, N., Gryczynski, I. , Gryczynski, Z. *Chem. Phys. Lett.* **434**, 326-330.

Depolarized light scattering from silver nanoparticles. Gryczynski, Z., Lukomska, J., Lakowicz, J.R., Matveeva, E.G., Gryczynski, I. (2006) *Chem. Phys. Lett.* 421, 189-192.

Phase difference of two resonances may exceed 90° in between, if they are enough far apart

The two components are in phase – resultant mainly in the direction of the electric field

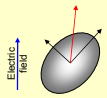

The two components are out of phase – resultant more perpendicular to the electric field

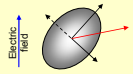

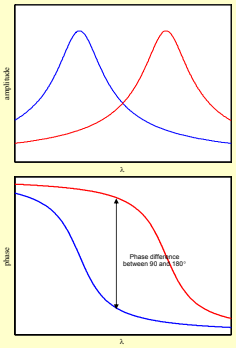

Estimating Scattering from Shape Distribution

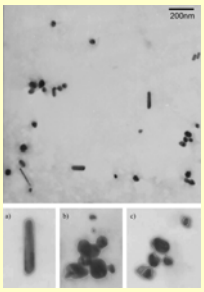

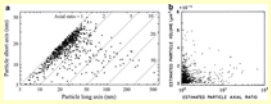

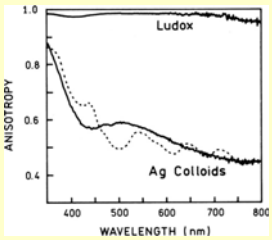

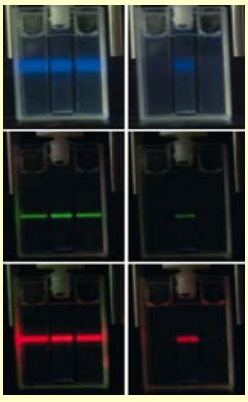

Wavelength-Ratiometric Scattering Sensor Based on Metallic Colloids

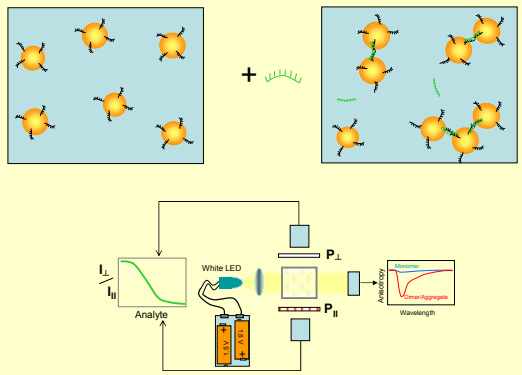

Metal Enhanced Fluorescence (MEF)

Metal Enhanced Fluorescence – Localized Plasmons

Light efficiently coupled in – stronger EM field – stronger excitation

Reciprocity – light efficiently coupled out – shorter lifetimes

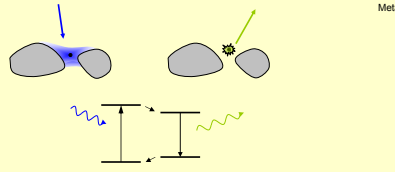

Fluorophore

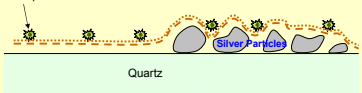

Quartz

Metal Enhanced Fluorescence (MEF)

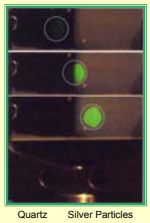

Quartz Silver Particles

Metal Particles Can Change the Radiative Decay Rates

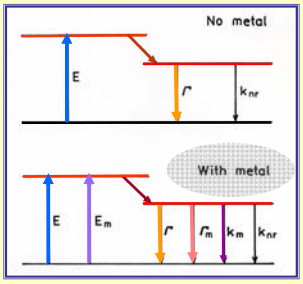

$Q_0 = \Gamma/(\Gamma + k_{nr})$

$Q_m = (\Gamma + \Gamma_m)/(\Gamma + \Gamma_m + k_{nr})$

$\tau_0 = 1/(\Gamma + k_{nr})$

$\tau_m = 1/(\Gamma + \Gamma_m + k_{nr})$

Metallic Surfaces can Create Unique Fluorophores with High Quantum Yields and Short Lifetimes

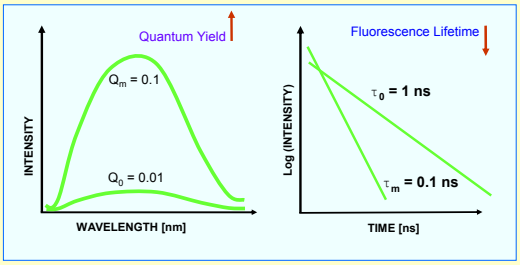

Sample on Planar Surface

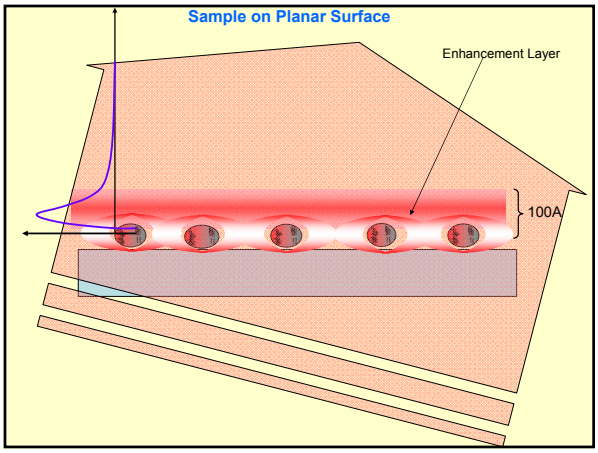

Fluorescence Immunoassays with Non-Fluorescent Chromophores

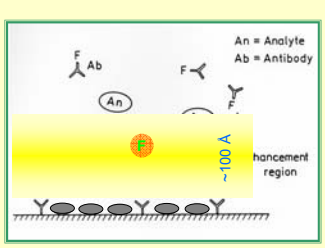

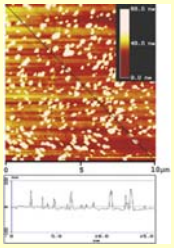

•Easy preparation
•Difficult to control

Intrinsic Emission from Unlabeled DNA

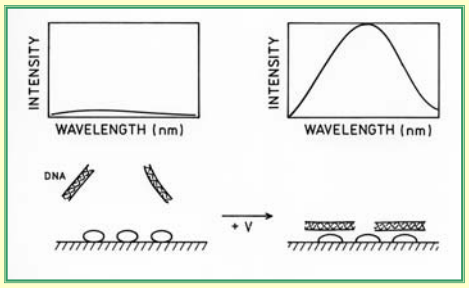

Emission Spectra of Double Helical DNA in the Presence and Absence of Silver Island Films

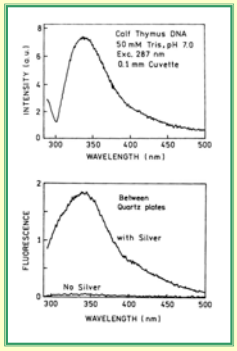

Frequency-Domain Intensity Decays of Double Helical DNA in the Absence and Presence of a Silver Island Film

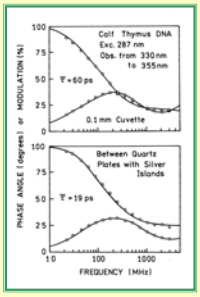

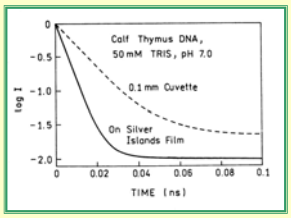

How Enhancement Depends on Distance ?

How to experimentally measure enhancement?

Distance Dependence of Enhanced Fluorescence of Cy3 and Cy5-Labeled Oligonucleotides

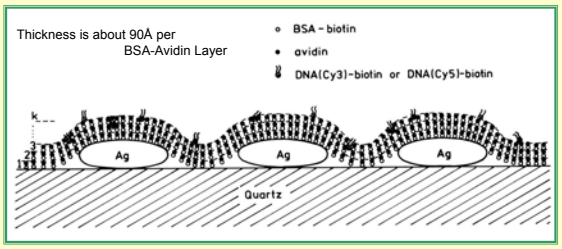

Absorption Spectra Show Complete Coverage for Each BSA-Biotin-Avidin Layer

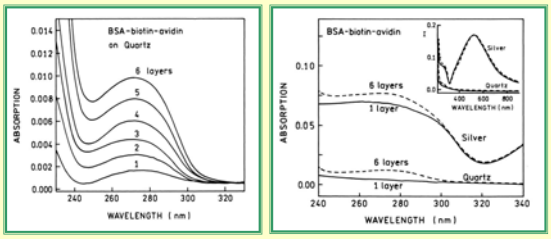

Dependence of Emission Intensity on Distance from Silver Particles

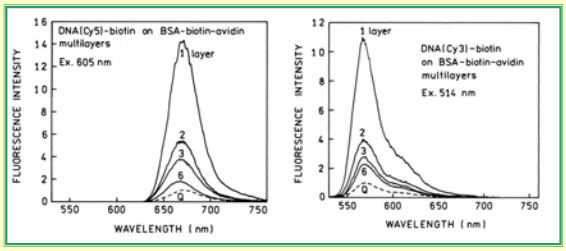

Shortest Lifetimes are Found for the Shortest Distance with BSA-Biotin-Avidin Layer

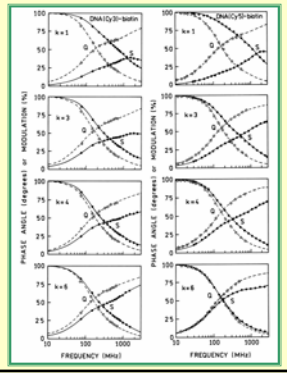

Relative Intensity and Lifetimes of DNA(Cy-dyes) on Quartz and SIFs

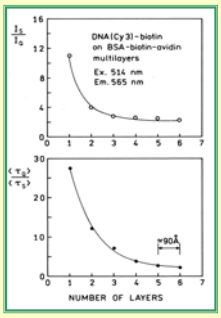

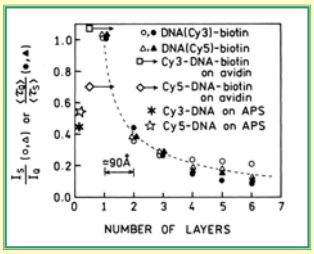

Model

Model

$A = A r_0\, e^{-d/d0} + 1$

$Q = N_r\, e^{-d/dq0} + 1$

Fitting Equations:

$$Gqy(d, Nr, Nnr, dy, dn) := \frac{\left(Nr\, e^{\frac{-d}{dy}} + 1\right)\cdot(\Gamma + knr)}{\left(Nr\, e^{\frac{-d}{dy}} + 1\right)\cdot\Gamma + \left[Nnr\, e^{\frac{(-d)^2}{dn}} + 1\right]\cdot knr}$$

$$Gt(d, Nr, Nnr, dy, dn) := \frac{\left(Nr\, e^{\frac{-d}{dy}} + 1\right)\cdot\Gamma + \left[Nnr\, e^{\frac{(-d)^2}{dn}} + 1\right]\cdot knr}{\Gamma + knr}$$

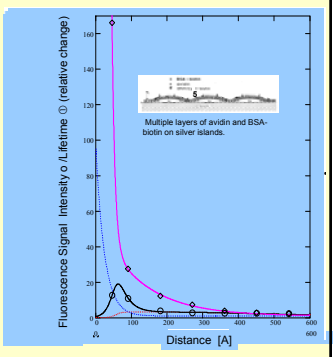

Distance Dependence of Excitation (ex) Radiation (r) and Non-Radiative (ns) Decay

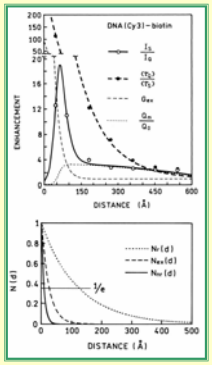

Fluorescent Properties Near Metal Particle

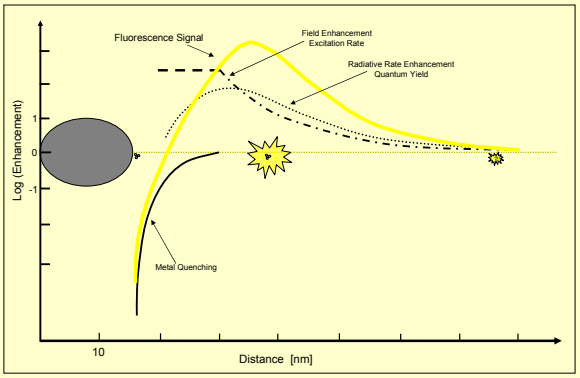

Fluorescence Enahancment is a Product of:
- Field
- Quantume Yield
- Quenching

How to separate field enhancement and quantum yield enhancement?

Application of MEF to Muscle Study

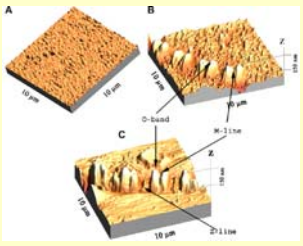

(A) AFM image of glass coated with SIF

(B) myofibrils on glass coverslips coated with SIF

(C) myofibrils on glass coverslips

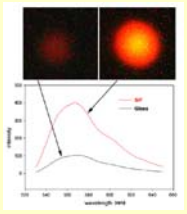

Enhancement of fluorescence by SIF. Myofibrils (1 mg/mL) labeled with 0.1 IM Rh-phalloidin were placed on a glass coverslip (top left) and on a coverslip coated with SIF (top right). The spectra were measured at a 45 angle in a Varian Eclipse spectrofluorometer. The vertical scale is in arbitrary units (a.u.). The spectrum of SIF in theabsence of muscle is less than 10 a.u. at all wavelengths.

Increased Brightness on SIFs

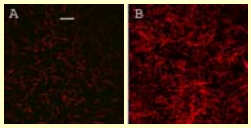

Confocal image of myofibrils contributing to the fluorescence of

(A) myofibrils on glass coverslip;

(B) myofibrils on glass covered with SIF. Bar is 10 lm. Exposure is the same in each panel.

Enhancement of fluorescence by SIF using TIR fluorescence. Myofibrils were placed on glass coverslip (left column) or on glass coverslips coated with SIF and detected by TIRF. The representative images, from the faintest to the most intense, are shown. Exposure times and camera gain are the same for each panel.

Decreasing Photobleaching by Silver Island Films: Application to Muscle

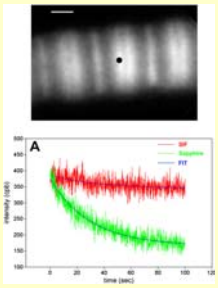

Comparison of the rate of photobleaching of the myofibrillar overlap zone on uncoated sapphire (green) and on sapphire coated withSIF (red)

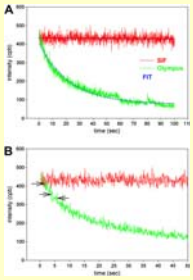

Comparison of the photobleaching of myofibrillar overlap zone on uncoated Olympus TIRF coverslips (green) and on Olympus TIRF coverslips coated with SIF (red)

Anal. Biochem. (2007) ***366,*** *228-236*

Ultra Bright Fluorophores for Multi-Photon Excitation

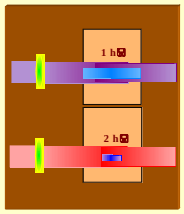

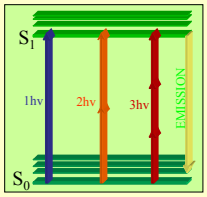

$$Q = \frac{\Gamma_r}{\Gamma_r + \Gamma_{nr}} \qquad \tau = \frac{1}{\Gamma_r + \Gamma_{nr}}$$

$$Q_m = \frac{N_f\Gamma_r}{N_f\Gamma_r + N_f\Gamma_{nr}} \qquad \tau_m = \frac{1}{N_f\Gamma_r + N_f\Gamma_{nr}}$$

$$G_{qy} = \frac{Q_m}{Q} = \frac{N_f(\Gamma_r + \Gamma_{nr})}{N_f\Gamma_r + N_f\Gamma_{nr}} \qquad G_\tau = \frac{\tau_m}{\tau} = \frac{\Gamma_r + \Gamma_{nr}}{N_f\Gamma_r + N_f\Gamma_{nr}}$$

$$G_p^{(1)} = G_{exc} \cdot G_{em} = G_{exc} N_f \frac{\tau_m}{\tau} \qquad G_p^{(2)} = G_{exc}^2 \cdot G_{em} = G_{exc}^2 N_f \frac{\tau_m}{\tau}$$

$$\frac{G_p^{(2)}}{G_p^{(1)}} = G_{exc}$$

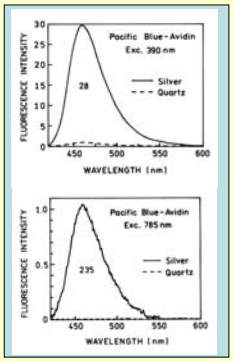

Table. Calculated enhancement factor for the labeled avidin

Probe	$G_p^{(1)}$	$G_p^{(2)}$	G_{exc}	$\Gamma(ns^{-1})^b$	$\Gamma_m(ns^{-1})^b$	N_f
Pacific Blue	28	235	25	0.32	11[c]	35
Lissamine	16	200[a]	9.5[a]	0.53	23[c]	45
Texas Red	46	200[a]	418[a]	0.16	71[c]	455

[a]Calculated assuming two-photon excitation displays a 200-fold increases in probe fluorescence on the silver island films.
[b]Calculated using $\Gamma = Q/\langle\tau\rangle$
[c]Calculated assuming the quantum yield Q = 1.0 on the silver island films

Conclusion

Picosecond Laser Diode Can Be Used for Two-Photon Excitation

Fluorescence Assays Utilizing MEF

HTS Format Assay

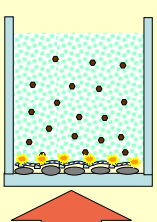

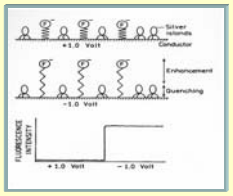

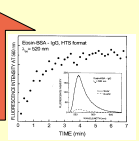

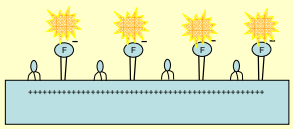

DNA Hybridization Can be Measured Using Silver – Enhanced Fluorescence

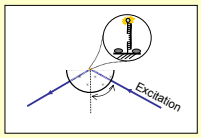

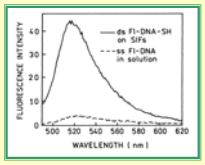

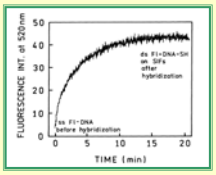

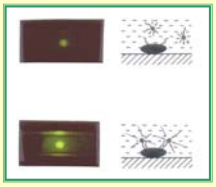

Use of surface plasmon-coupled emission to measure DNA hybridization (2004). Malicka J., Gryczynski I., Gryczynski Z., Lakowicz J.R., J. Biomol. Screening, **9**(3), 208-215.

TIRF Immunoassay on a Silver Island Surface

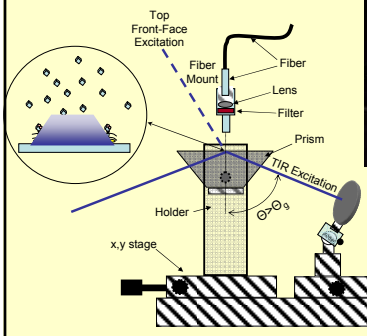

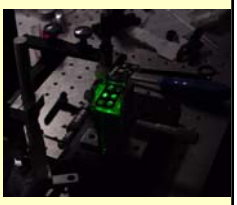

Mirror

Metal-enhanced fluorescence immunoassays using total internal reflection and silver island-coated surfaces (2004). Matveeva E., Gryczynski Z., Malicka J., Gryczynski I., Lakowicz J.R., *Anal. Biochem.*, **334**, 303-311.

Coupled plasmon effects for the enhancement of fluorescent immunoassays. (2007) Anne Barnetta, Evgenia G. Matveevaa, Ignacy Gryczynskia, Zygmunt Gryczynskia, Ewa M. Goldys. *Physica* B. **394**, 297–300

Scanning Confocal System. Capability of Separating 500 nm Spots

What maximum enhancement to expect ?

Can We Do Immunoassay on a Single Molecule Level ?

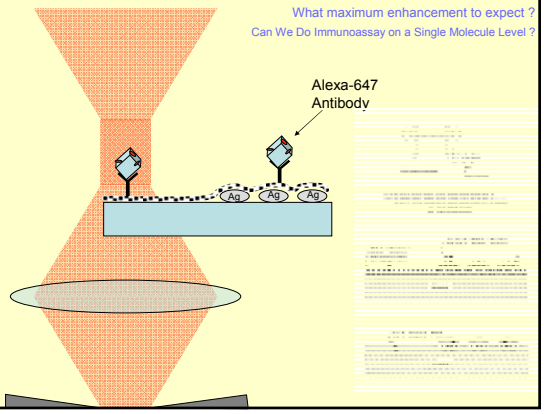

Monolayer of Labeled Antibodies

On Glass
(Intensity Scale 0-10)

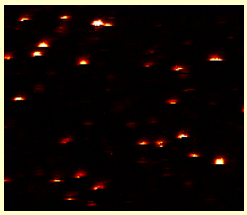

On Silver Island Film
(Intensity Scale 0-100)

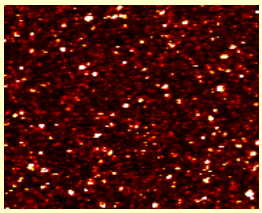

Future of Biomedical Assays – Assay Based on Single Molecule

Alexa647 c=1pg/ml **GLASS** λ=635nm Filter HQ685nm/70

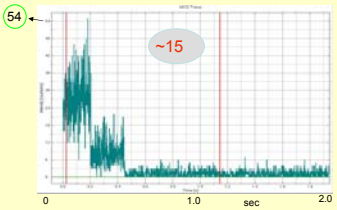

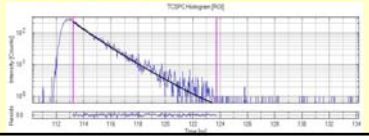

Ampl. 1	140.59
Lifet. 1	1.777
Ampl. 2	82.2
Lifet. 2	0.968
Backgr.	0.16

Alexa647 c=1pg/ml **SILVER** λ=635nm Filter HQ685nm/70

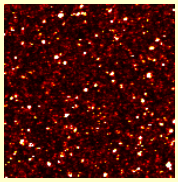

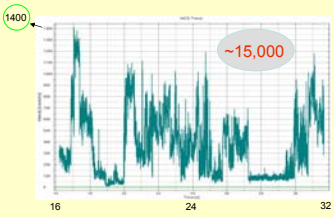

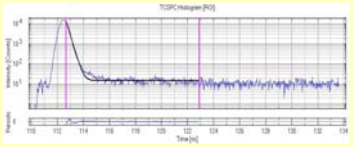

Ampl. 1	13360.91
Lifet. 1	0.201
Backgr.	14.5

Assay Based on Nanostructures and Microfluidics

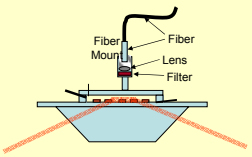

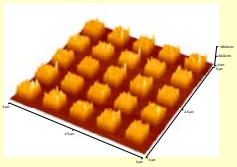

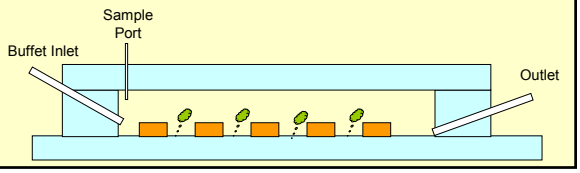

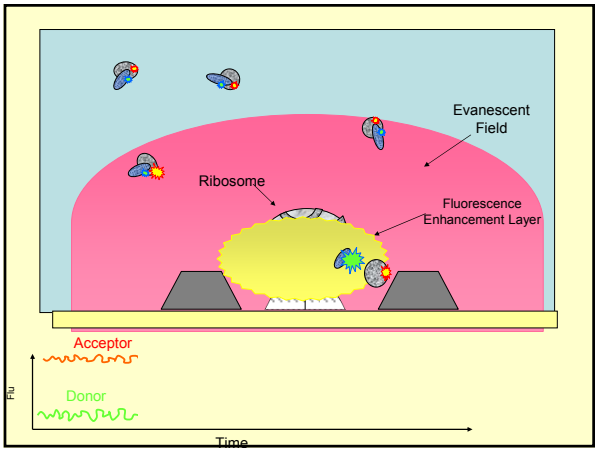

Fluorescence Enhancement on Silver Electrochemical Deposition

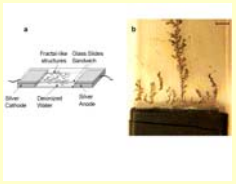

a)The sandwich set-up for electrochemical growth of silver fractal-like structures on glass slides.

b) The photo of the glass slide with grown silver fractal-like structures. The bar on top is 6 mm in length.

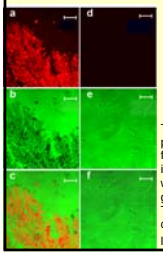

The laser scanning confocal microscope images. The images of the immunoassay performed on glass slides with fractal-like structures (left column) and without fractal-like structures (right column). (**a**) The fluorescence images of the immunoassay prepared on the glass slide with fractal-like structures and (**d**) without the fractals. (**b**) The transmission images of the immunoassay made on the glass slide with fractal-like structures and (**e**) without the fractal-like structures. (**c**) The superimposed fluorescence and transmittance images of the immunoassay carried out on the glass slide with fractal-like structures and (**f**) without the fractal-like structures. The bars on all images represent 50 mm.

Fluorescence Enhancement on Silver Fractal-Like Structures

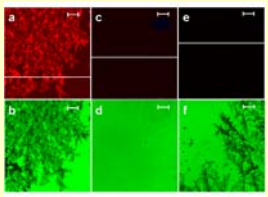

High magnification laser scanning confocal microscope images:

(a) the fluorescence images of the immunoassay prepared on the glass slide with fractal-like structures,

(c) the immunoassay prepared on a clean glass slide, and

(e) a non-specific binding performed on a glass slide with fractal-like structures.

(b) The images in transmission mode of the immunoassay prepared on the glass slide with fractal-like structures,

(d) on a clean glass slide,

(f) on a glass slide with fractal-like structures with non-specific protein binding.

The bars on all images represent 5 mm.

Fluorescence Enhancement on Silver Fractal-Like Structures

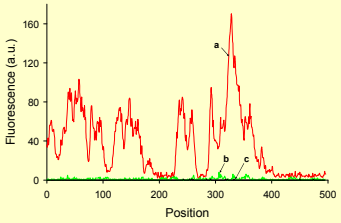

Comparison of the fluorescence emission signals

(a) The fluorescence intensities due to the immunoassay measured at the cross-section of the glass slide with fractal-like structures shown in Figure 4a as a white line.

(b) The fluorescence intensities due to the immunoassay measured at the cross-section of the clean glass slide shown in Figure 4c as a white line.

(c) The fluorescence intensities due to non-specific binding measured at the cross-section of the glass slide with fractal

JACS (2007) ***129****, 12117-12122*
Anal. Biochem. (2008) ***in press***

CCFT

SPCE

New Concept of Fluorescence

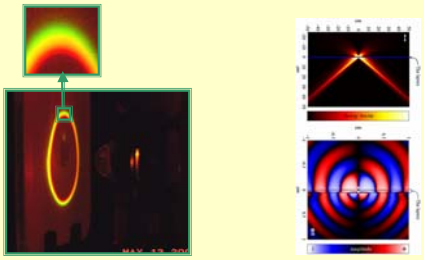

Wavelength resolution of SPCE

Surface Plasmons

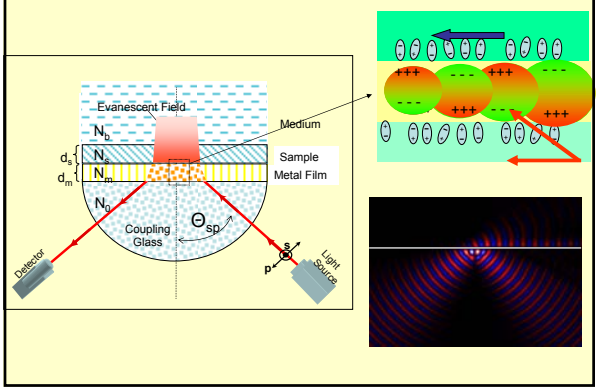

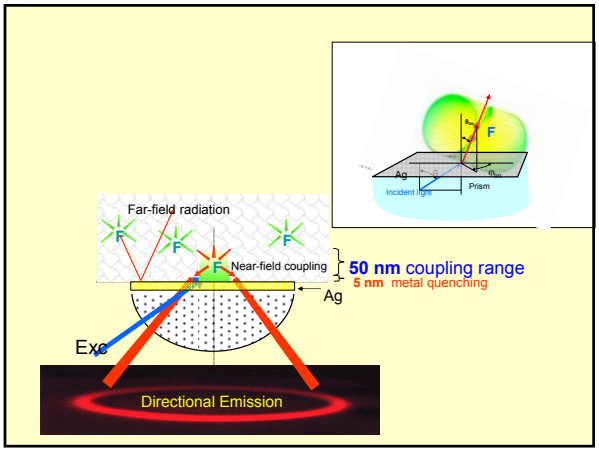

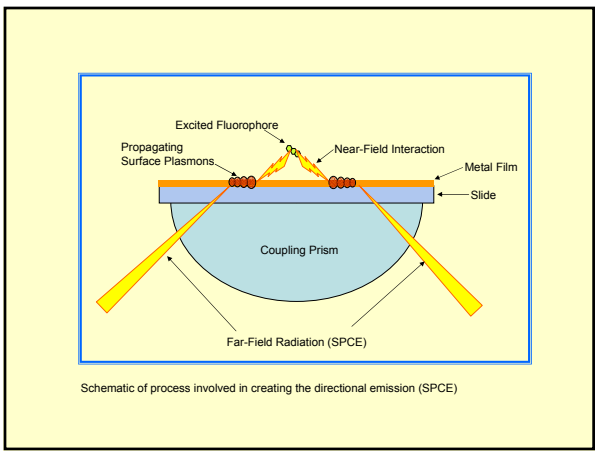

Schematic of process involved in creating the directional emission (SPCE)

Examples of SPCE - Different Metals

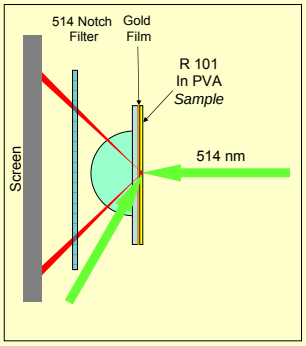

Surface-plasmon-coupled emission: New technology for studying molecular processes. Gryczynski Z., Gryczynski I., Matveeva E., Malicka J., Nowaczyk K., Lakowicz J.R., in Cytometry: New Developments (Methods in Cell Biology, Vol. 75) 4th edition, Darzynkiewicz Z., Roederer M. and Tanke H.J. (Eds), Academic Press, 2004, pp. 73-104

SPCE Angular Dependence

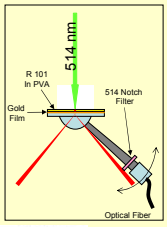

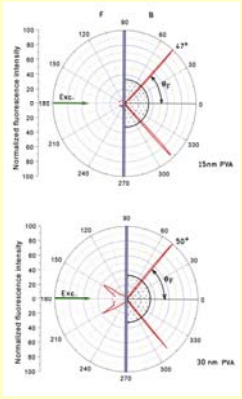

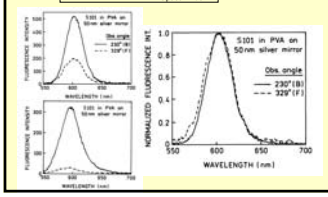

Mixture of Fluorophores – Wavelength Resolution

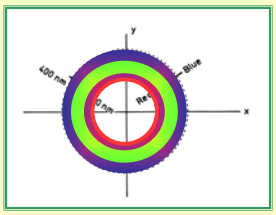

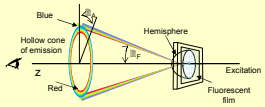

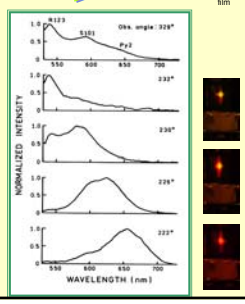

Radiation Diagrams

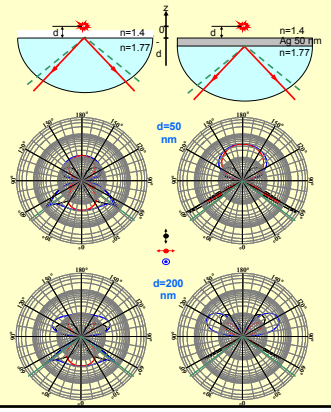

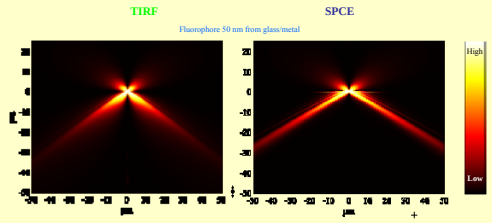

Calculated Reflectance and Electric Fields TIR and SPR Conditions
What is the Effective Distance from the Interface

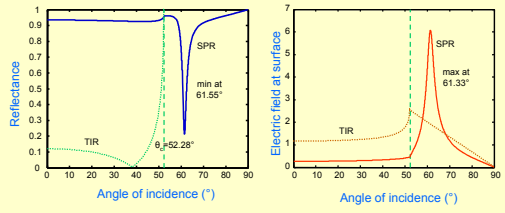

Effective Depth Penetration for SPCE

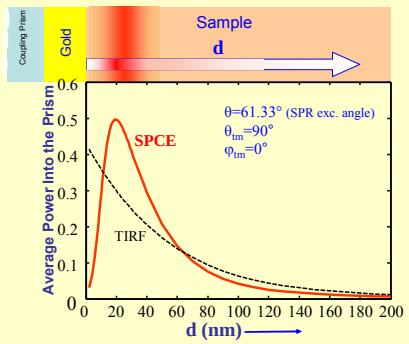

Surface Plasmon Assisted Microscopy (SPAM)

Effective Volume

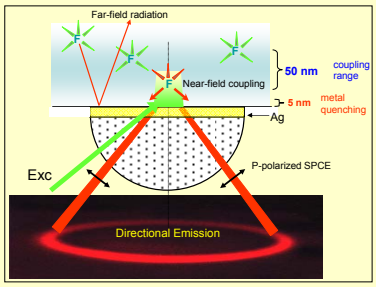

Concept of surface plasmon-coupled emission (SPCE). F is a fluorophore. The excitation energy of fluorophore couples to the surface plasmons and radiates to the glass prism in form of the ring. Far-field radiation is reflected by the metal surface.

Fluorescence Immunoassays on Surface

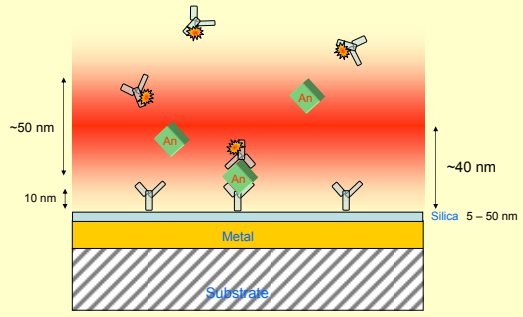

SPCE-based Assays

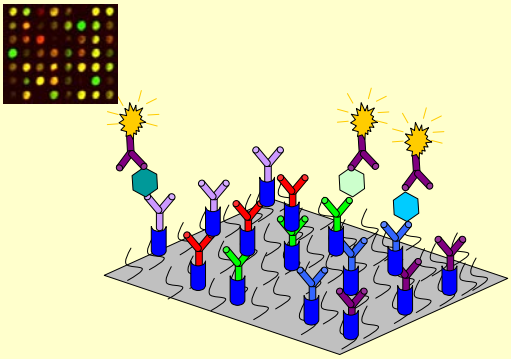

Model Immunoassay with SPCE

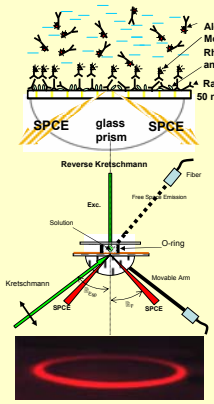

Myoglobin immunoassay utilizing directional surface plasmon-coupled emission (2004).Matveeva E., Gryczynski Z., Gryczynski I., Malicka J., Lakowicz J.R., *Anal. Chem.*, **76**, 6287-6292.

Directional Surface Plasmon-Coupled Emission – Application for an Immunoassay in Whole Blood. Matveeva E.G., Gryczynski Z., Malicka J. Lukomska J., Makowiec S., Berndt K.W., Lakowicz J. R., Gryczynski I. (2005). *Anal. Biochem.*, 344(2), 161-167.

How to Minimize Excitation Volume

- The observational volume of conventional wide-field microscopes is way too large. For example, in 1 cm long muscle cell there are ~100 billion myosins in the typical observational volume. Even if we observe with diffraction limited optics (high NA objective, laser illumination) the number of observed molecules is ~million.
- The introduction of small observational volumes defined by confocal detection made it possible to limit the thickness to few micrometers (2-3 μm) and eliminate much background (confocal microscope).
- Two-photon (2P) microscope can reduce the thickness by factor of 2 but this is still too large to define a single molecule.

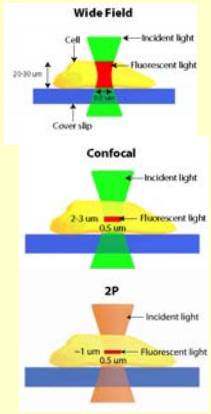

Number of observed molecules

These ideas are summarized in the Table. The experimental volume is the volume seen with diffraction-limited optics. The numbers are based on number of myosin molecules in skeletal muscle (so called myosin bridges, xbs).

Method	Exp volume (L)	~# of xbs in the volume	Degree of labeling (%)	~# of observed (fluorescent) xbs
Wide field	10^{-14}	10^{6}	100	10^{6}
Confocal	$0.3x10^{-15}$	$2x10^{4}$	2	400
2P	$0.2x10^{-15}$	10^{4}	2	200
TIRF/Con	$4x10^{-18}$	200	2	4

A new method is required !!!

- The method described here, a combination of Surface Plasmon Coupled Emission (SPCE) and confocal microscopy (referred to here as Confocal SPCE) offers hope to see a single molecule in a cell.
- The principle is shown schematically at right. The light which impinges on a silver-plated cover-slip made from sapphire at SPR angle, penetrates the silver and resonates with surface plasmons to create extremely bright fluorescence (~50 x brighter than fluorescence excited by TIR).

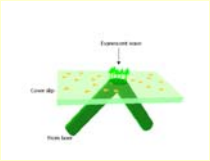

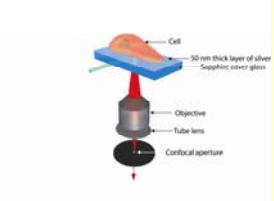

Principle of the method

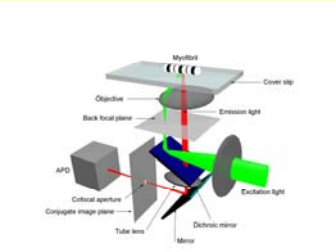

Method	Experimental volume (L)	~Number of xbs in the volume	Degree of labeling (%)	~Number of observed (fluorescent) xbs
SPCE	10^{-18}	100	2	2

Principles of SPCE Microscopy

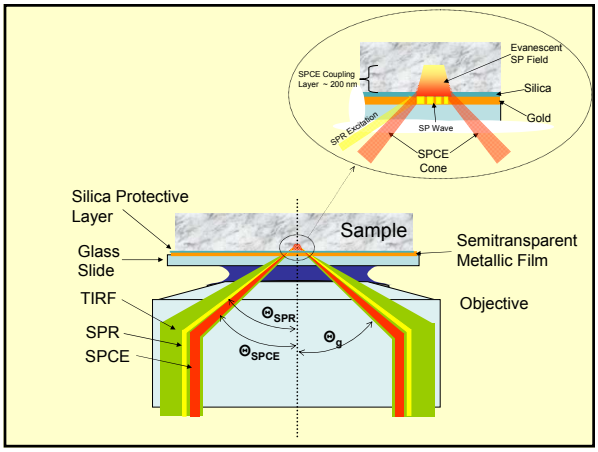

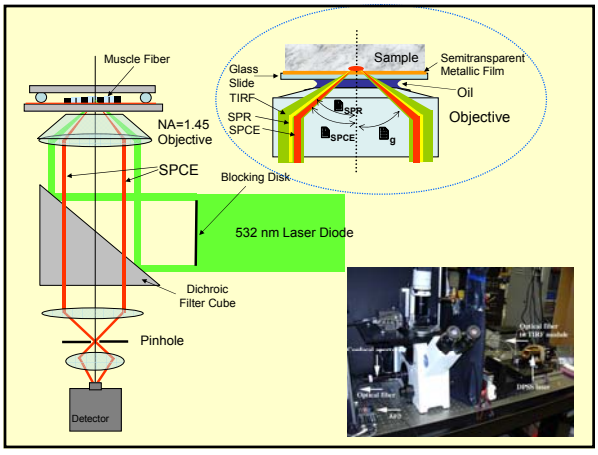

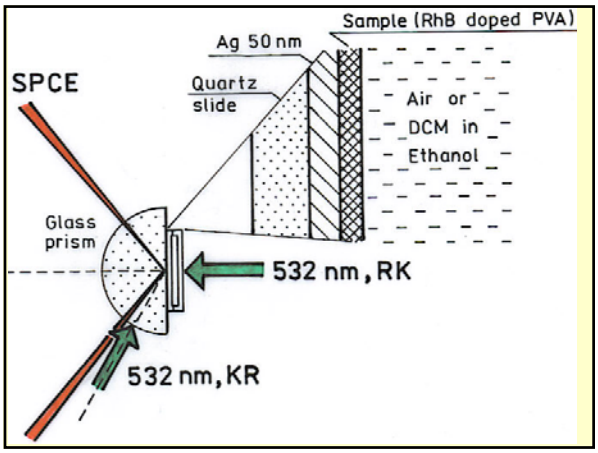
Sample (RhB doped PVA)
Ag 50 nm
SPCE
Quartz slide
Air or DCM in Ethanol
Glass prism
532 nm, RK
532 nm, KR

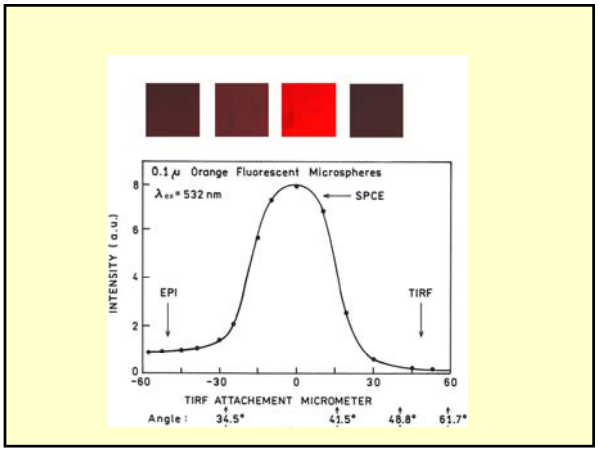
0.1 μ Orange Fluorescent Microspheres
λex = 532 nm
SPCE
EPI
TIRF
INTENSITY (a.u.)
TIRF ATTACHEMENT MICROMETER
Angle : 34.5° 41.5° 48.8° 61.7°

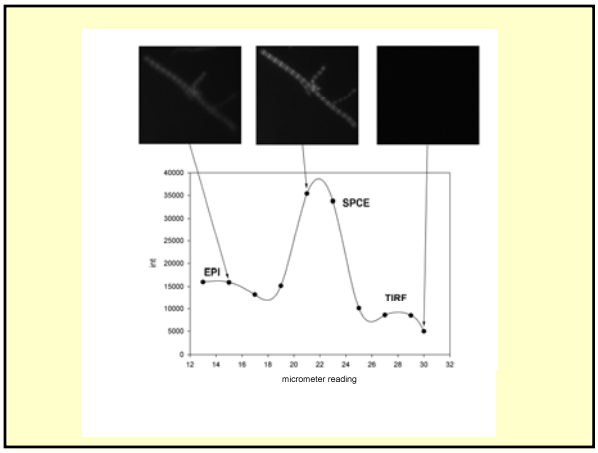
SPCE
EPI
TIRF
micrometer reading

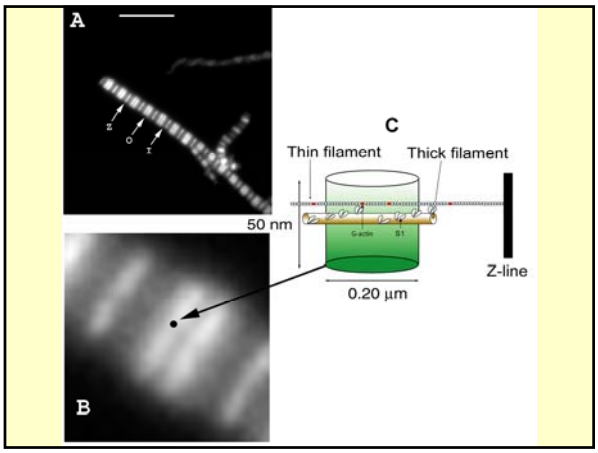

Muscle, cntd

Confocal SPCE signal from rigor myofibril. The data was collected from the overlap zone. Myofibril labeled with 0.1 µM rhodamine-phalloidin on gold coverslips. The exciting light was perpendicular to the plane of coverslip (p-polarization).
A: Fluorescence intensity.
B: intensity on expanded scale, gray-original signal, red-low pass filtered.

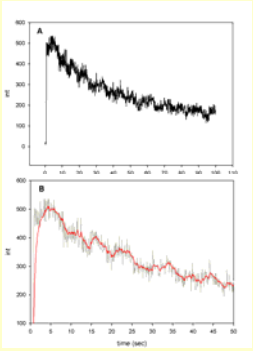

Photostability

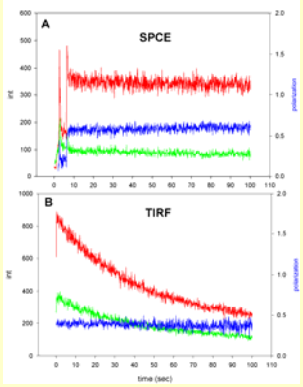

???

FCS with Surface Plasmons

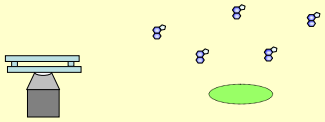

$$G(t) = 1 + \frac{1}{2N}\frac{\sum_{m=-\infty}^{\infty} d_m d_{m-n} A_m A_{m-n} R_{m-n}(t)}{\sum_{m=-\infty}^{\infty} d_m d_{m-n} A_m A_{m-n}}$$

$$R_{m-n}(t) = \left(1+\frac{Dt}{\sigma^2}\right)^{-1}\left(1-\frac{2Dt}{d_x^2}\right)\mathrm{erfc}\left(\sqrt{\frac{Dt}{d_x^2}}\right)\exp\left(\frac{Dt}{d_x^2}\right) + \sqrt{\frac{4Dt}{\pi d_x^2}}$$

$$R_{m-n}(t) = \left(1+\frac{Dt}{\sigma^2}\right)^{-1}\left(\frac{d_m}{d_m - d_n}\mathrm{erfc}\left(\sqrt{\frac{Dt}{d_m^2}}\right)\exp\left(\frac{Dt}{d_m^2}\right) + \frac{d_n}{d_n - d_m}\mathrm{erfc}\left(\sqrt{\frac{Dt}{d_n^2}}\right)\exp\left(\frac{Dt}{d_n^2}\right)\right)$$

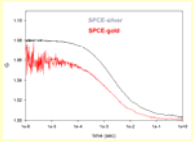

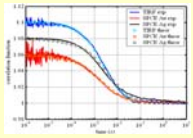

Fluorescence Correlation Spectroscopy in Surface Plasmon Coupled Emission Microscopy. (2006) Borejdo, J., N. Calander, Z. Gryczynski, and I. Gryczynski. *Optic Express*. 14. (17), 7878-7888.

Another Interesting Property of SPCE

Waveguide Assisted SPCE

SPR – Salomon and Tolin

SPCE from Thick and Thin PVA Films

Effects of Film Thickness on the Angular Distribution of SPCE

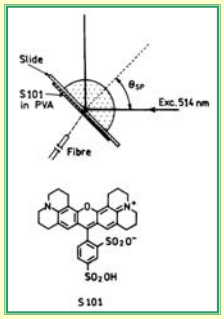

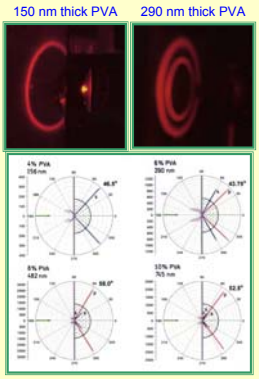

p & s Ring Polarization

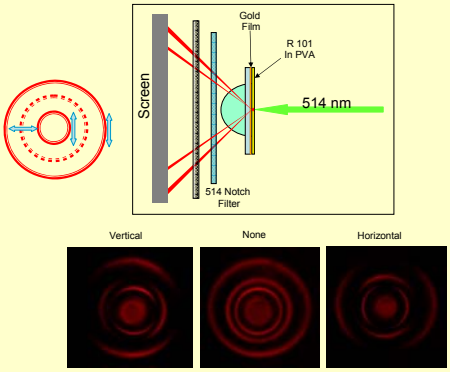

Model Hybridization Assay with SPCE

Ratiometric Detection of Wavelength Resolved SPCE

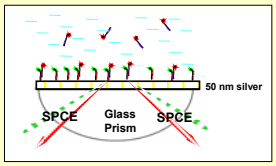

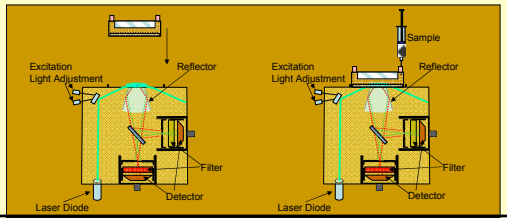

Effect of Orientation of Emitting Dipole

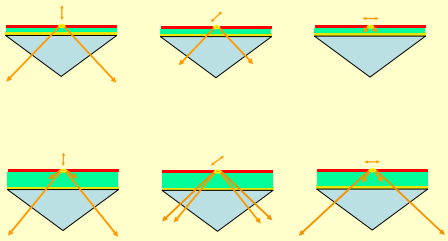

Studying Conformational Dynamics

Process that Involve Conformational Change

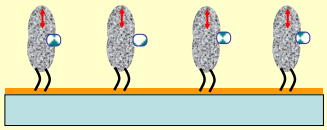

Utilizing the Waveguide Technology

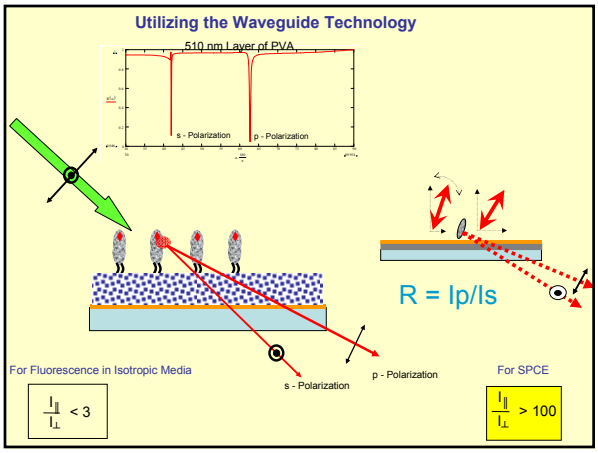

Theoretical Calculation

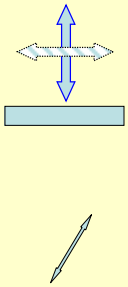

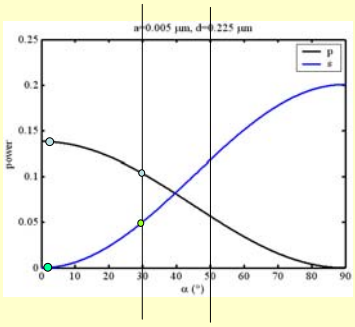

Power flow of p-polarized (black) and s-polarized light versus dipole angle ><.

SPCE Microscope - Tool For Direct Detection of Conformational Changes

Conformational Change Upon Ligand Binding

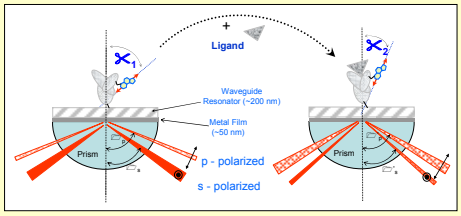

A schematic description of conformational change occurring upon ligand binding.
We will detect bounding (mass change), conformational change (reorientation of the binding side), and by time-resolved measurement change in the protein mobility (if induced by binding).

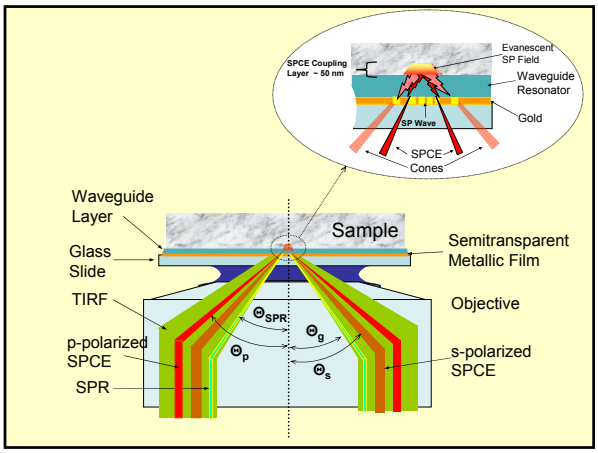

Schematic Concept for Waveguide Assisted SPCE Microscope

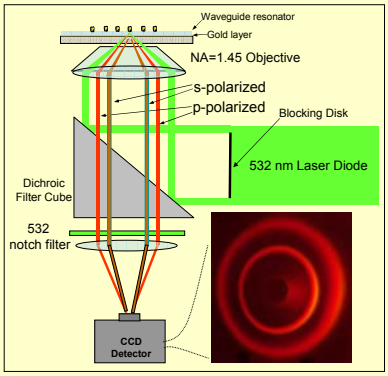

SPCE From Single Horizontal Dipole
What about in plane rotations?

Molecular Motion in Azimuthal Angle

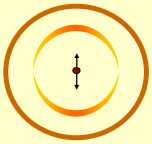

A Model System

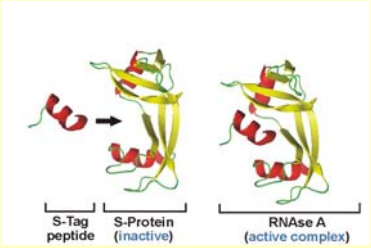

Interactions between protein pairs in bovine pancreatic ribonuclease A (RNase A). The structure of the crystalline protein is rendered as cartoon depicting the secondary structural elements with helices colored red, sheets colored yellow and random coils colored green. A) Cleavage of the N-terminal 15 amino acids of RNase A produces what is called an S-Tag peptide and an enzymatically inactive protein called S-protein. B) The high affinity binding of the S-Tag peptide to the inactive S-Protein forms a bimolecular complex with RNase activity.

Acknowledgment

Emerging Technology Fund of Texas
National Institute of Health (NIBIB & NCI)
National Science Fundation
BITC
Philip Morris External Research Program

CCFT Team
Ignacy Gryczynski
Julian Borejdo
Ben Harris
Nils Calander
Evgenia Matveeva
Irina Akopowa
Gabor Laczko
Tanya Shtoyko
Ralal Luchowski
Mariusz Szabelski
John Talent

Students

Priya Mathu
Sashank Bharil
Pabak Sakar
Prassad Yala Maticola